4D printing of Porous PLA-TPU Structures: Effect of Applied Deformation, Loading Mode and Infill Pattern on the Shape Memory Performance

To cite this article before publication: Davood Rahmatabadi *et al* 2023 *Phys. Scr.* in press https://doi.org/10.1088/1402-4896/ad1957

4D printing of Porous PLA-TPU Structures: Effect of Applied Deformation, Loading Mode and Infill Pattern on the Shape Memory Performance

Davood Rahmatabadi[a], Kianoosh Soltanmohammadi[a], Mohammad Aberoumand[a], Elyas Soleyman[a], Ismaeil Ghasemi[b], Majid Baniassadi[a], Karen Abrinia[a], Mahdi Bodaghi[c*] and Mostafa Baghani[a*]

[a] *School of Mechanical Engineering, College of Engineering, University of Tehran, Tehran, Iran*

[b]*Faculty of Processing, Iran Polymer and Petrochemical Institute, Tehran, Iran*

[c]*Department of Engineering, School of Science and Technology, Nottingham Trent University, Nottingham NG11 8NS, UK*

[*]*Corresponding authors: mahdi.bodaghi@ntu.ac.uk; baghani@ut.ac.ir*

Abstract

For the first time, the synergy of shape memory polymer (SMP) blending, 4D printing, and cold programming (CP) are investigated for improving the functionality of the shape memory effect (SME), increasing medical applications of porous structures, direct programming, and removing current limitations. Porous PLA-TPU structures with different printing patterns and applied deformation were CPed under constrained and non-constrained compression modes at room temperature and were recovered in the rubbery phase. The shape fixity and shape recovery ratios were calculated and the cross-section morphology was examined with scanning electron microscopy (SEM). The shape fixity values were in the range of 39.75-71.27%, while almost complete shape recovery ratios (100%) were observed for all porous samples. Low shape fixity ratios can be justified due to the existence of two steps of spring-back and structure relaxation after unloading in cold programming, resulting from elastic and viscoelastic behavior. The glass transition temperature of the PLA-TPU blend was 69 °C and shifted to raw materials, indicating the possibility of some interaction between the two components. SEM images showed the uniform distribution of TPU particles and matrix-droplet morphology in the PLA-TPU blend. After printing, TPU droplets were stretched and the sea-island morphology was observed in some segments.

Keywords: PLA-TPU; Shape memory polymers; 4D-printing; Material extrusion; Porous structure; Cold programming.

1- Introduction

Shape memory polymers (SMPs) are one of the novel and widely used polymers in the category of smart materials that can save the secondary shape and return to the original shape in the face of a suitable stimulus [1–4]. This feature, called the shape memory effect (SME) is not one of the inherent properties of polymers and is a combination of morphology, structure, and programming that can lead to an SME [5–7]. For this reason, pure thermoplastics which have the SME are limited to several materials, including Poly Lactic Acid (PLA) and Polyurethane (PU) [8–10]. Poly Lactic Acid (PLA) is a very attractive polymer for use in various applications due to its biocompatibility properties, but its brittleness has led to limitations that require additional operations [11,12]. As mentioned, one of the most important parts of the SME is programming, which is often done at high temperatures (in the rubbery region), which is called hot programming (HP) [5]. HP, in addition to higher cost (energy and time), saves and recovers less force, and due to the limitations of polymers in force recovery compared to metals, these factors further limit the use of SMPs and now have created a new challenge for researchers to directly programming at ambient temperature [13]. HP includes the stage of heating, loading, cooling, and unloading, but in contrast, Cold Programming (CP) only includes loading and unloading. CP requires the application of high deformation to the thermoplastic in the glassy region, where most polymers are brittle and require additional operations such as polymer blending which has received more attention than polymerization, due to a lower cost and a simpler process in designing and manufacturing SMPs [5,13]. Porous shape memory polymers are the new generation of SMPs and can have wide potential applications in aerospace, medicine, and other industries [14,15] . For example, in medical applications, the presence of cavities with controlled sizes, in addition to providing conditions for internal growth, can also be a gateway for transferring

body fluids [16–19]. PLA filament reinforced with magnesium metal particles was successfully produced, and its printability by material extrusion technique and use for porous scaffolds were investigated. Or they can improve the shape memory performance of temperature-stimulated polymers (recovery rate), due to higher permeability [16,20]. Various methods have been proposed for the fabrication of porous SMPs such as gas-forming, electrospinning, and 3D printing [21,22]. Nowadays, 3D printing as a new method without limitations in design and construction has also created the ability to produce controllable and regular porous structures that have some advantages such as the ability of complex geometries, reproducibility and predictability of properties as well as better mechanical performance due to lack of local stress concentration due to non-uniform distribution of cavities compared to random porous structures produced by the traditional methods [18,23–26]. Therefore, with the expansion and development of additive manufacturing technology, the applications of related fields such as smart materials have increased, and researchers continue to try to remove obstacles [27,28]. Fused Deposition Modeling (FDM) as a subset of the Material extrusion (MEX) method is the simplest and cheapest 3D printing technology, the mechanism of which is the extrusion of molten filament on the bed and the underlying layers based on the digital design file [29–31]. The combination of MEX and CP (direct programming) by reducing and saving time and cost and adding the capability of complex and porous geometries can increase the medical applications of 4D printing [32–34].

In this study, for the first time, the topics of SMP blending, printing porous structures, and cold programming, which are the three main sides of 4D printing, are investigated to improve the functionality of shape memory, increase the medical applications of porous structures, and direct programming and removing its limitations. For this purpose, PLA was blended with 30 wt% of Thermoplastic Polyurethane (TPU) to add cold programming

capability by applying high deformations at room temperature. Porous structures with an infill density of 20% and different patterns were printed and cold programmed under two applied deformations, both constrained and unconstrained loading. Dynamic Mechanical Thermal Analysis (DMTA) and Scanning Electron Microscopy (SEM) imaging were also used to characterize thermal analysis and morphology.

2- Materials and methods

2-1- Materials

In this research, PLA and TPU granules were used as raw materials. Due to its low formability at ambient temperature, PLA does not have the ability to be cold programmed (deformation and strain applied beyond the elastic zone). For this reason, it is necessary to use a plasticizer such as TPU for PLA in order to increase the formability. On the other hand, due to its good compatibility with PLA, TPU can be added up to 50% by weight. But due to the fact that increasing the amount of TPU above 30% causes the formation of co-continuous and sea-island morphologies and also the elastic part of the SMP is strongly strengthened, it destroys the achievement of the desired shape fixity value in cold programming. For this purpose, PLA-TPU (70-30) composition was chosen considering the increase of PLA formability and preventing excessive loss of shape fixity in cold programming.

The porous printed parts were prepared in several steps, including the melt mixing of granules with a weight percentage of 70 to 30 PLA and TPU in the internal mixer, fabrication of thin sheets using a hot press, crushing and preparation of PLA-TPU granules, extrusion and fabricating filament to print the final samples. PLA-TPU blend with 30% TPU by weight was prepared by melt mixing in an internal mixer at 190°C and 60 rpm for 10 minutes. Then, in two stages of hot and cold pressing, the sheets were

prepared and by crushing them, the granules of PLA-TPU blend were prepared. The transformation of granules into filament with a diameter of 1.75 mm was done with a laboratory extruder at a temperature of 200°C and 25 rpm.

2-2- 3D printing

The porous PLA-TPU structures were printed with a cross-section of 20×10 mm and a height of 10 mm and a 20% infill density (80% porosity) and three lozenges, vertical and horizontal patterns with a MEX 3D printer with an accuracy of 0.1 mm. The printing parameters are presented in Table 1. The equipment, filament, and printed sample are presented in Figure 1.

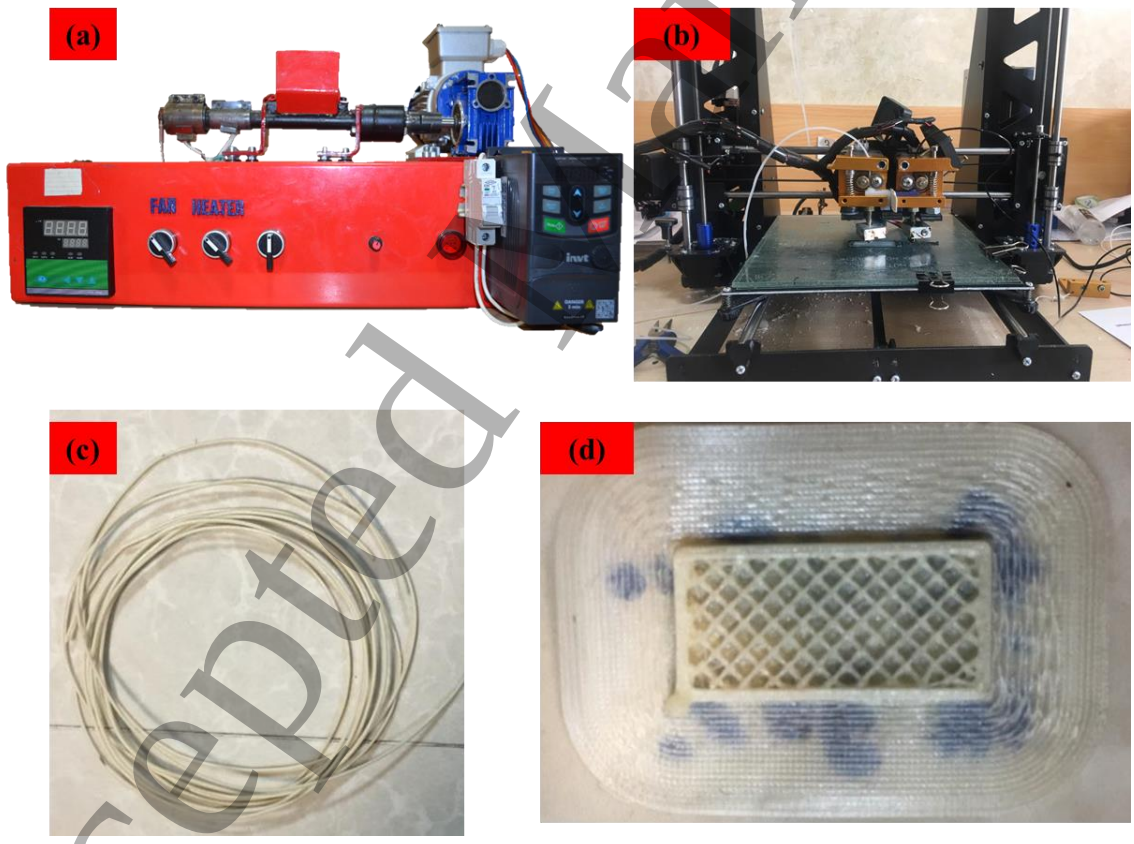

Figure 1. (a) extruder, (b) FDM 3D printer, (c) filament, and (d) printed sample.

2-3- Shape memory cycle

The programming and recovery steps were conducted by a customized servo-mechanical universal tensile test machine equipped with a temperature-controlled liquid chamber, designed and manufactured by Khallagh Sanat Atieh Peyman Company. Programming and recovery conditions according to Table 2 were considered the same for all samples. Programming in compression mode was performed by applying axial deformation to reduce only the volume (using the mold to prevent the increase of cross-section) and free deformation by applying two deformations (40% and 80%) at room temperature. For each condition, the shape memory cycle was repeated at least three times. Free deformation is common in performing shape memory cycling in different loading modes. But the use of constrained and guided deformation method by a mold is done for various applications such as smart packaging with automatic opening capability to reduce volume. The shape fixity and shape recovery ratio were measured according to Eqs 1-2 and Figure 2, which A, B, C and D are the initial height, the amount of deformation, the height after unloading, and recovery, respectively. Shape recovery was also done for all samples under the same conditions.

$$shape\ fixity\ ratio = \frac{B}{A - C} * 100 \quad (1)$$

$$shape\ recovery\ ratio = \frac{A - C}{D - C} * 100 \quad (2)$$

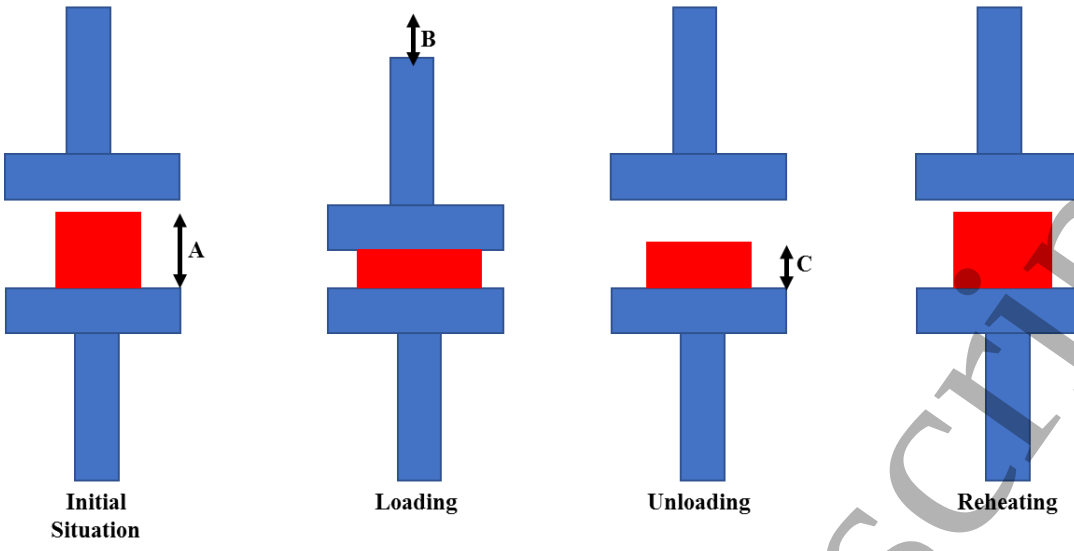

Figure 2. Schematic explanation for different stages of shape memory cycle and calculation of shape fixity and shape recovery parameters in compression loading mode

Table 1: Printing parameters

Bed temperature	50 °C
Nozzle temperature	210 °C
Velocity	30 mm/s
Number of shells	2
Nozzle diameter	400 µm
Layer thickness	200 µm
Infill density	20%
Pattern	Horizontal/Vertical and Lozenge

Table 2: Programming, and recovery parameters

Programming temperature	25 °C
Recovery temperature	80 °C
Heating rate	15 °C/min
Cooling rate	30 °C/min
Deformation rate	3 mm/min
Deformation	4 and 8 mm

2-4- DMTA and SEM

To study the thermomechanical behavior and determine the different thermal zones of the PLA-TPU blend, the dynamic mechanical thermal analysis (DMTA) test was done by a dynamic mechanical thermal analyzer (Mettler Toledo, Switzerland). Imaging was also done by a scanning electron microscope (SEM) to study the bond quality between the PLA-TPU layers and the effect of 3D printing on the morphology by PhilipsXL30 SEM.

3- Results and discussion

3-1- DMTA

Figure 3 shows the DMTA results for PLA and TPU as raw materials and their combinations PLA-TPU. The middle of loss storage modulus for raw materials was considered as the transition temperature. According to Figure 3(a) ans 3(b) PLA and TPU have glass transition temperatures of 74°C and -30°C, respectively. Based on Figure 3(c), the glass transition temperatures of the PLA-TPU blend is 69°C and shift to raw materials, indicating the possibility of some interaction between the two components. These interactions may be due to some intermolecular interactions between the PLA molecular chains and the soft elastomeric parts of TPU [35,36]. The compound has two peak in the loss modules at -12°C and 71°C, which are correspond to the TPU and PLA phases. The presence of two Tan delta peaks at the transition temperature of the ingredients of the PLA-TPU indicates an immiscible blend. The strongest intensity of the peak at 71°C is due to the higher weight percentage of PLA. In addition, the storage modulus of PLA-TPU decreases compared to PLA and the addition of TPU reduces and increases the values of storage and loss modulus, respectively. In the glass transition temperature range, the storage modules of the compounds suddenly decrease due to softening of the composition and more freedom of movement and mobility of the polymer chains.

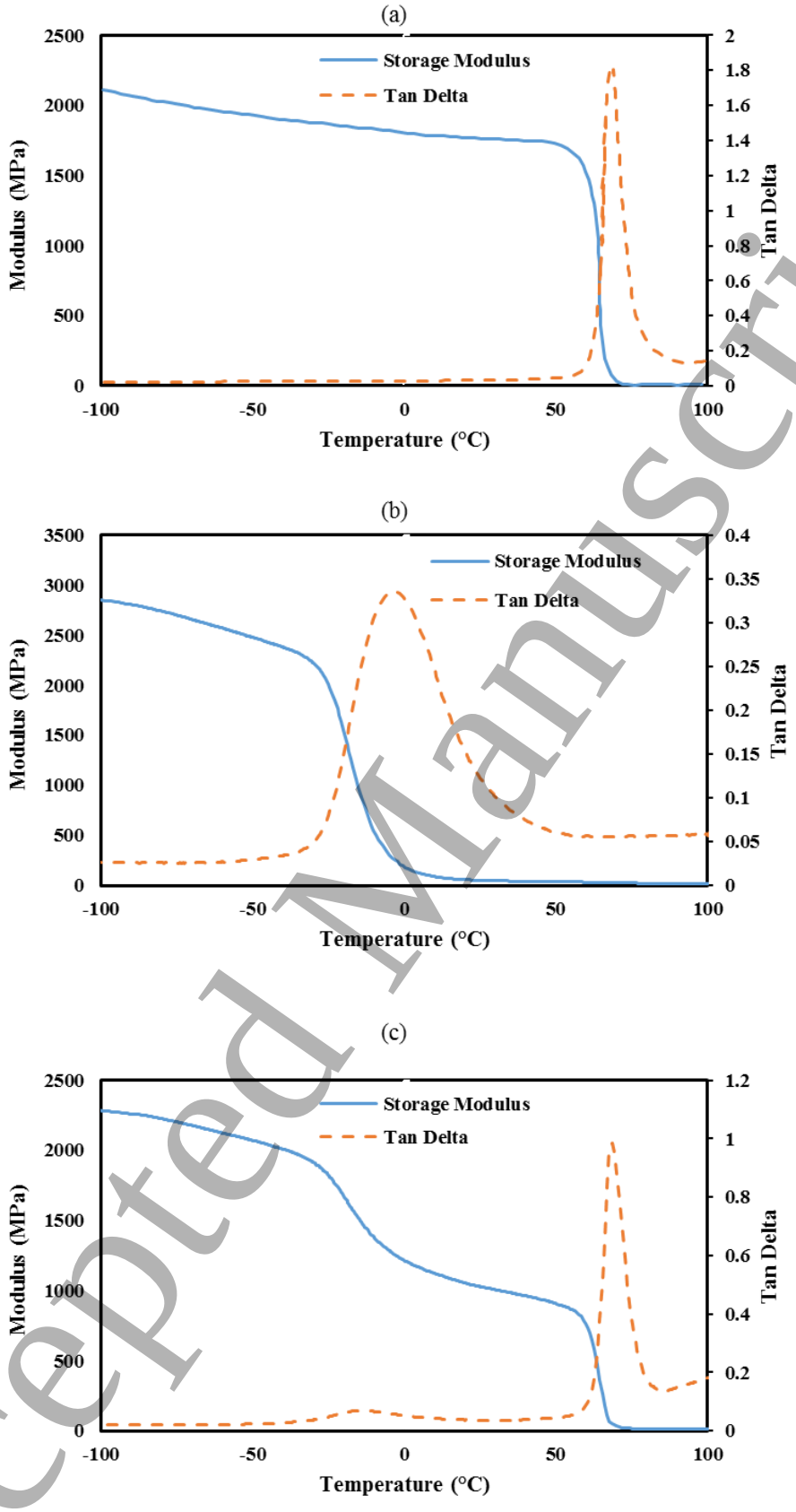

Figure 3. DMTA results of: (a) PLA, (b) TPU, and (c) PLA-TPU.

3-2- shape memory effect

As mentioned in the previous section, shape memory properties, including shape fixity and shape recovery, were investigated for three patterns, two applied deformation, with two free and constrained mechanisms. The schematic of the shape memory tests is presented in Figure 4. The constrained shape memory test was carried out for all three patterns with a special mold with the same dimensions as the porous sample to prevent cross-section deformation for packaging and medical applications. As can be seen, the deformation mechanism during programming is different in the two shape memory tests, and in the constrained state, the walls buckle inwards due to the constraints created by the mold, while in the free state, most of the walls undergo bending.

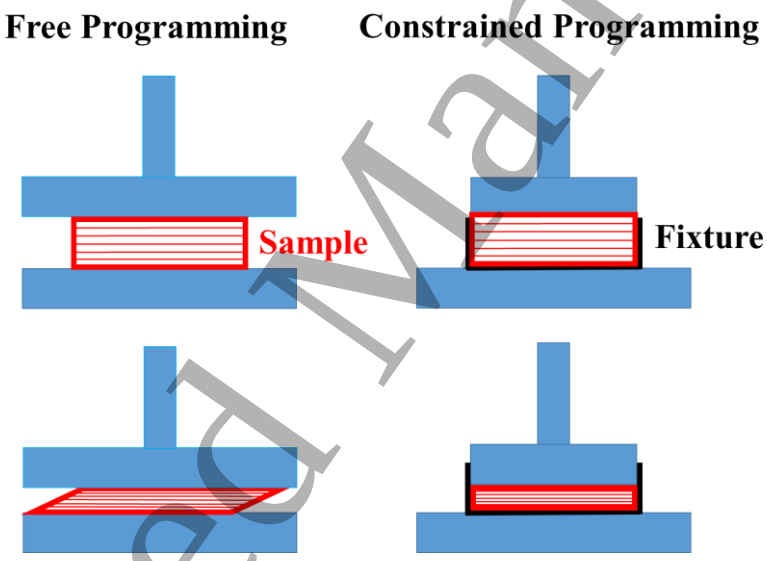

Figure 4. A schematic illustration of free and constrained shape memory tests.

In Figures 5 and 6, the original, programmed and recovered examples for three horizontal, vertical and lozenge patterns are shown in the constrained state. In addition to the mentioned cases, in the constrained state, it is possible to compress the infill at a high applied deformation. Also, the behavior of the vertical walls (in the direction of applying force) in 40% and 80% deformation after recovery is different in both patterns and the

40% applied samples are completely recovered, while with the doubling of the deformation, due to plastic buckling, the walls are not completely restored. These results are strongly related to the plastic instability in the loading mode and the applied deformation.

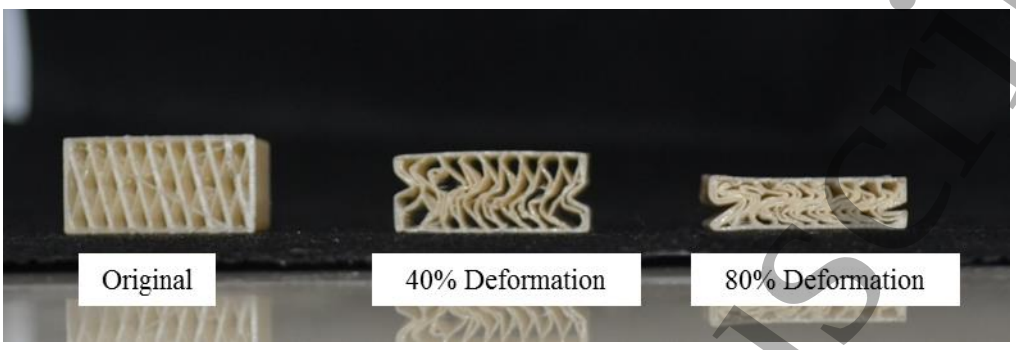

Figure 5. Programmed samples in terms of the constrained applied defomation

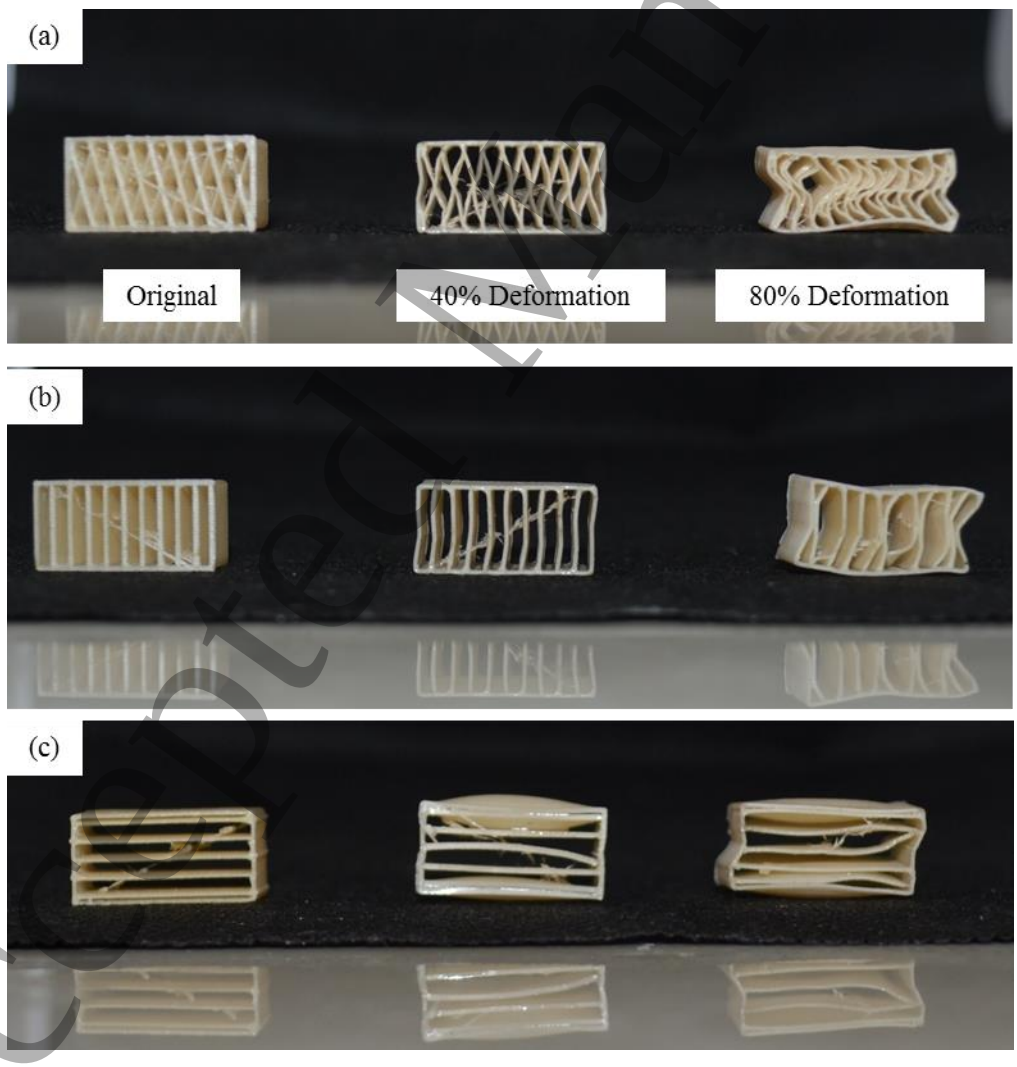

Figure 6. Original and recovered samples in terms of the printing pattern under 40% and 80% constrained applied programming: (a) lozenge pattern, (b) vertical, and (c) horizontal patterns.

In Figures 7 and 8, the shape fixity values of the three printing patterns, two applied deformation values for the unconstrained and constrained, respectively are presented. According to these figures, the amount of shape fixity has increased with the increase of the applied deformation, and the effect of the deformation is more intense and more than the other two parameters. Also, quantitive results of shape fixity for porous PLA-TPU blend in terms of printing pattern, programming deformation, and loading mode is summarized in Table 3. Shape fixity values for all samples are in the range of 39.75 to 71.27%, which is due to CP, part of the deformation is recovered quickly and over time, which is due to elastic and viscoelastic recovery, respectively [13]. In fact, CP includes two stages of elastic recovery and structure relaxation after unloading [5]. For this reason, the polymer must have high deformability (higher than yield) at ambient temperature (glass region) that can be directly programmed. Because after unloading, the amount of elastic strain returns quickly and the viscoelastic term of the strain also returns over time and only a part of the plastic strain can be stabilized. In the thermodynamic equilibrium state, polymer chains are helical and randomly distributed. By increasing the amount of strain (beyond the linear and yielding region), the polymer chains are stretched towards the loading direction, and in this way, they are separated from their equilibrium state. By increasing the applied load or keeping the polymers in a stretched state, more instability is created in the polymer equilibrium system [37]. For this reason, the value of shape fixity is higher for more deformed samples.

The results show that all three parameters are effective on shape fixity so that with increasing applied deformation, the shape fixity ratio increases, and the maximum amount of fixity is obtained for the unconstrained compressive loading mode compared to

constrained samples. By doubling the amount of applied deformation during CP (from 40% to 80%), the shape fixity values for the unconstrained state increased by 1.47, 1.41, and 1.52 times, for vertical, horizontal, and lozenge patterns, respectively. As the results confirm, in CP, the amount of applied strain is an essential parameter because, in this process, the amount of strain must be higher than the yield strain to improve the fixity capacity. In CP, the increase in internal energy and local plastic strains cause temporary shape stabilization, and elastic and viscoelastic strains are released immediately after unloading and time-dependent, respectively [5,13]. Also, the effect of the printing pattern is different in the two loading modes, and in the unconstrained and constrained modes, the highest shape fixity ratios have been obtained for lozenge and horizontal patterns, respectively. In fact, the effect of loading mode and printing pattern on shape fixity is related to the thermodynamic stability of the polymer, and these factors cause more chains to contribute to the local plastic deformation. Free deformation compared to constrained provides more freedom of action to the chains to move towards higher density voids, which have higher stabilization capability.

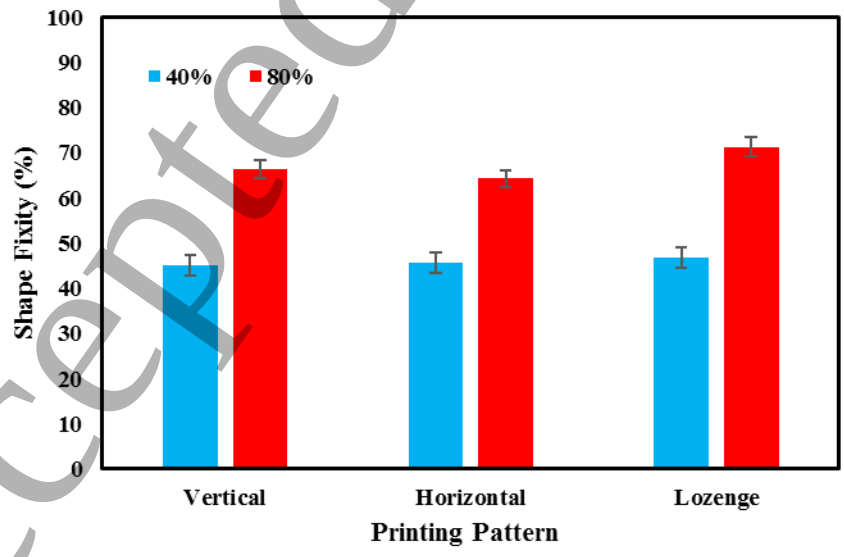

Figure 7. Shape fixity results in terms of the printing pattern and applied deformation for unconstrained mode

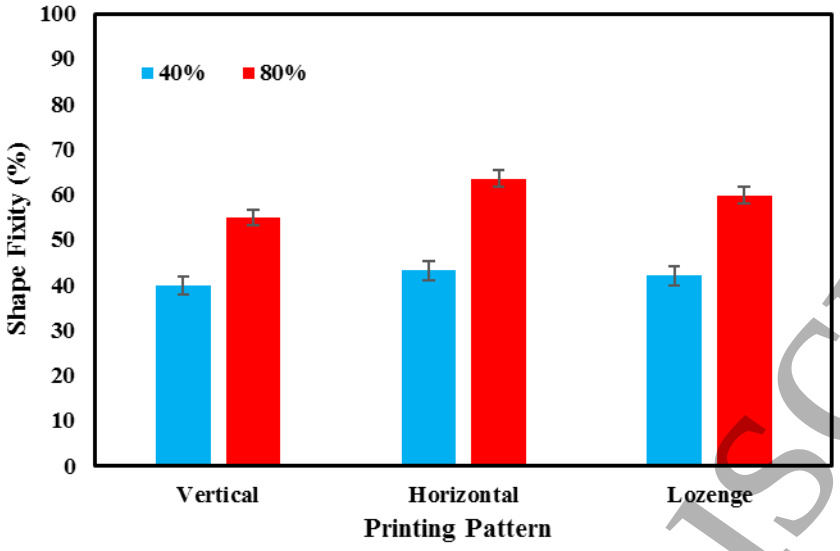

Figure 8. Shape fixity results in terms of the printing pattern and applied deformation for constrained mode

Table 3. Shape fixity results in terms of the printing pattern and programming deformation

Deformation / Printing pattern	Shape Fixity Ratio			
	40%		80%	
	Unconstrained	Constrained	Unconstrained	Constrained
Vertical	45.11±2.39	39.75±1.51	66.27±2.69	54.86±1.85
Horizontal	45.67±3.01	43.21±2.25	64.32±±2.83	63.52±2.11
Lozenge	46.84±2.09	42.05±2.96	71.27±2.19	59.77±2.40

After the unloading stage was done, the porous PLA-TPU samples were heated and after reaching the recovery temperature, the shape recovery value was measured. The results of this study are presented in Figures 9 and 10. The quantitive shape recovery results are also sammurized in Table 4 in terms of the printing pattern and programming deformation, in which according to the results, the dependence of the recovery ratio on the studied parameters is much less than shape fixity. Complete shape recovery (100%)

is observed for both constrained and unconstrained and all three printing patterns at 40% applied strain, but at higher applied deformation (80%), lozenge pattern, and constrained loading showed higher shape recovery ratios. As mentioned in the previous section, the applied strain includes three parts: elastic, viscoelastic, and plastic. Viscoelastic and plastic strains are stored locally in a segment with weaker and stronger constraints (areas with more and less free volume), respectively [5,38]. Therefore, at low applied strain, fewer parts with rigid constraints undergo local deformation and are released more easily and quickly by applying heat. In addition, even though more instability caused an increase in shaoe fixity values in the previous stage, it causes more energy to be needed to return to the equilibrium and stable state. According to the same recovery conditions (time and temperature), the samples that have a greater distance from their thermodynamic equilibrium state have a weaker recovery performance [39,40].

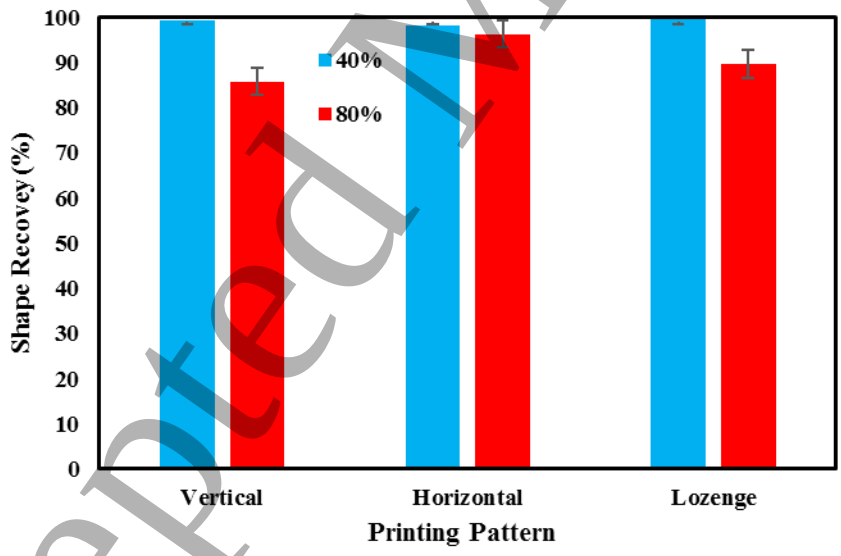

Figure 9. Shape recovery results in terms of the printing pattern and applied deformation for unconstrained mode

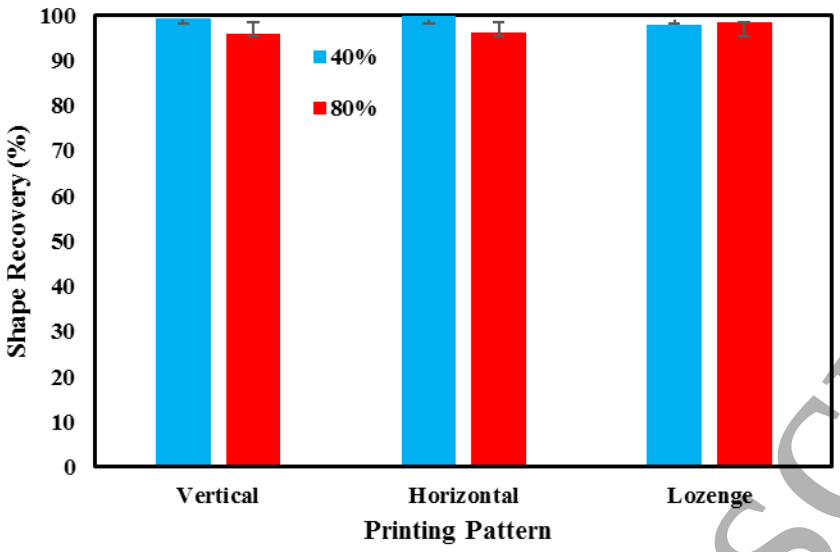

Figure 10. Shape recovery results in terms of the printing pattern and applied deformation for constrained mode

Table 4. Shape recovery results in terms of the printing pattern and programming deformation

	Shape Recovery Ratio			
Deformation / Printing pattern	40%		80%	
	Unconstrained	Constrained	Unconstrained	Constrained
Vertical	99.43±0.41	99.20±0.25	85.84±3.45	95.97±1.39
Horizontal	98.29±0.67	100±0	96.33±1.85	96.15±1.52
Lozenge	99.61±0.24	98.01±0.59	89.68±2.36	98.56±0.98

3-3- Microstructure evaluation

Figure 11 demonstrates the SEM images of the cross-sectional filament and printed PLA-TPU blend. According to Figures 11(a) and 11(b), a uniform distribution of TPU particle and matrix-droplet morphology is observed. In fact, the SEM images confirm the DMTA results that the PLA and TPU are compatible with each other and their blend is not miscible. Figure 11(d) shows microvoids and cavities due to incomplete melting, and insufficient adhesion of 3D-printed layers. These voids are the main cause of porosity in MEX 3D printed parts and it is believed that their complete elimination is impossible [41–43], because the rasters cool down very quickly and complete integration (crack

growth) does not take place [44]. Of course, the printing parameters that affect the feeding rate also play a role in the geometry and number of these holes [43,45]. In the 3D printed sample, the morphology of the matrix-droplet changes somewhat, and in Figure 11(e), parts of the TPU with the island's morphology are identified, that are formed by joining and stretching of the TPU droplets due to extrusion during printing.

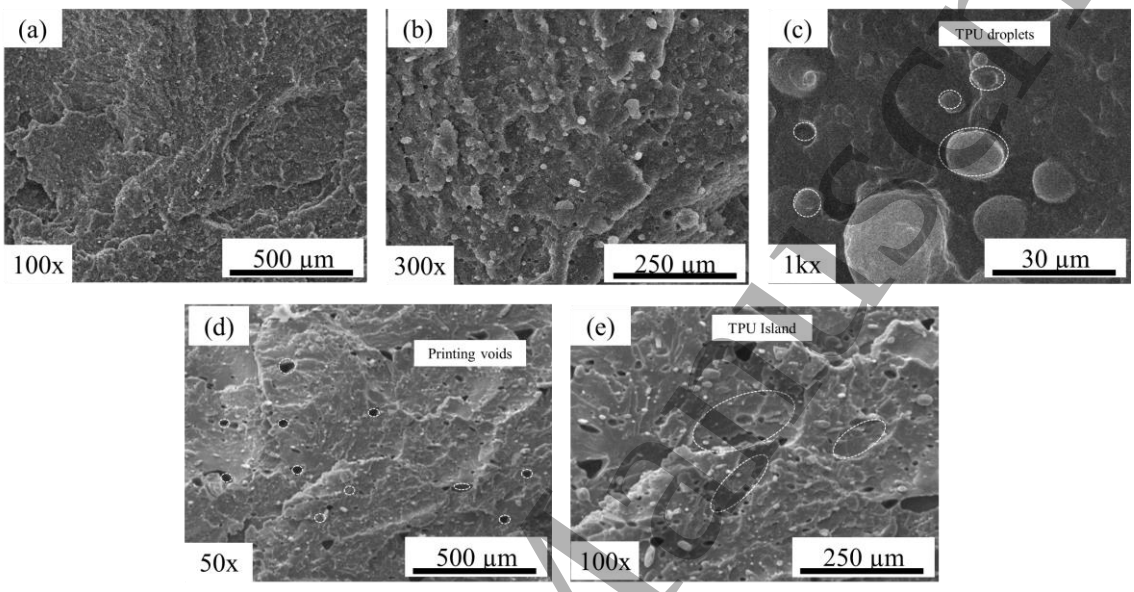

Figure 11. SEM images of PLA-TPU: (a-c) filament, (c) and (d) printed samples

4- Conclusion

In this pioneering research, the fusion of 3D printing, smart materials, and programming within the domain of 4D printing was investigated to enhance the capabilities of shape memory materials, particularly for their medical applications. The study commenced with the formulation of a PLA-TPU blend (70-30 wt.%) to improve shape memory performance and ductility at ambient temperatures while accommodating high deformations. Ordered porous specimens with horizontal, vertical, and lozenge patterns were successfully 4D printed for streamlined processing. To expedite experimentation, the specimens were programmed at ambient temperatures, and recovery within the rubbery region was observed. Comprehensive assessments, including thermal

analysis, microstructure evaluations, and shape memory property analyses, were conducted via constrained and free thermo-mechanical shape memory cycles, DMTA, and SEM. The following remarks can be drawn:

- Interactions between PLA and TPU components were identified through DMTA, as indicated by the shift in the glass transition temperature of the PLA-TPU blend. Compressive shape memory properties, particularly shape fixity, were influenced by various factors, including printing patterns, applied deformation, and loading modes. Shape fixity values ranging from 39.75% to 71.27% were observed, reflecting the interplay between elastic and viscoelastic recovery processes.
- At an applied strain of 40%, complete shape recovery (100%) was achieved across all three printing patterns, both constrained and unconstrained. However, at higher deformations (80%), superior shape recovery ratios were exhibited by the lozenge pattern and constrained loading.
- SEM analysis revealed a transition in filament morphology from matrix-droplet in raw material to a combination of matrix-droplet and sea-island structures in printed samples. Importantly, the findings highlight the promise of cold programming, encompassing only loading and unloading, coupled with 3D printing of smart materials for medical applications requiring intricate, porous, and personalized geometries. This approach not only reduces costs but also offers a time-efficient solution.
- In summary, the study unveiled the exciting potential of 4D printing in shaping the future of shape memory materials, especially in the realm of personalized and complex medical applications. The importance of tailoring printing parameters and material compositions to optimize performance was underscored, opening new avenues for innovative healthcare solutions.

References

1. Zafar, M.Q.; Zhao, H. 4D Printing: Future Insight in Additive Manufacturing. *Met. Mater. Int.* **2020**, *26*, 564–585, doi:10.1007/s12540-019-00441-w.
2. Wang, C.; Kou, B.; Hang, Z.; Zhao, X.; Lu, T.; Wu, Z.; Zhang, J.P. Tunable Shape Recovery Progress of Thermoplastic Polyurethane by Solvents. *Pigment Resin Technol.* **2018**, *47*, 7–13, doi:10.1108/PRT-03-2017-0021/FULL/XML.
3. Aberoumand, M.; Soltanmohammadi, K.; Rahmatabadi, D.; Soleyman, E.; Ghasemi, I.; Baniassadi, M.; Abrinia, K.; Bodaghi, M.; Baghani, M. 4D Printing of Polyvinyl Chloride (PVC): A Detailed Analysis of Microstructure, Programming, and Shape Memory Performance. *Macromol. Mater. Eng.* **2023**, *308*, 2200677, doi:10.1002/mame.202200677.
4. Aberoumand, M.; Rahmatabadi, D.; Soltanmohammadi, K.; Soleyman, E.; Ghasemi, I.; Baniassadi, M.; Abrinia, K.; Bodaghi, M.; Baghani, M. Stress Recovery and Stress Relaxation Behaviors of PVC 4D Printed by FDM Technology for High-Performance Actuation Applications. *Sensors Actuators A Phys.* **2023**, *361*, 114572, doi:10.1016/J.SNA.2023.114572.
5. Li, G.; Wang, A. Cold, Warm, and Hot Programming of Shape Memory Polymers. *J. Polym. Sci. Part B Polym. Phys.* **2016**, *54*, 1319–1339, doi:10.1002/polb.24041.
6. Soleyman, E.; Aberoumand, M.; Soltanmohammadi, K.; Rahmatabadi, D.; Ghasemi, I.; Baniassadi, M.; Abrinia, K.; Baghani, M. 4D Printing of PET-G via FDM Including Tailormade Excess Third Shape. *Manuf. Lett.* **2022**, *33*, 1–4, doi:10.1016/j.mfglet.2022.05.002.
7. Chen, L.; Li, W.; Liu, X.; Zhang, C.; Zhou, H.; Song, S. Carbon Nanotubes Array Reinforced Shape-Memory Epoxy with Fast Responses to Low-Power Microwaves. *J. Appl. Polym. Sci.* **2019**, *136*, 47563, doi:10.1002/APP.47563.
8. Kechagias, J.D.; Vidakis, N.; Petousis, M. Parameter Effects and Process Modeling of FFF-TPU Mechanical Response. *Mater. Manuf. Process.* **2021**, doi:10.1080/10426914.2021.2001523.
9. Benecke, L.; Tonndorf, R.; Cherif, C.; Aibibu, D. Influence of Spinning Method on Shape Memory Effect of Thermoplastic Polyurethane Yarns. *Polym. 2023, Vol. 15, Page 239* **2023**, *15*, 239, doi:10.3390/POLYM15010239.
10. Ye, W.; Dou, H.; Zhang, D.; Yang, F.; Cheng, Y.; Cai, W. Effects of Process Parameters on Mechanical Properties and Interface of 3D Printed Bamboo-Inspired CCFR-PLA/TPU Composites. *Polym. Compos.* **2023**, doi:10.1002/PC.27770.
11. Mehrpouya, M.; Gisario, A.; Azizi, A.; Barletta, M. Investigation on Shape Recovery of <scp>3D</Scp> Printed Honeycomb Sandwich Structure. *Polym. Adv. Technol.* **2020**, *31*, 3361–3365, doi:10.1002/pat.5020.
12. Demirtaş, M.S.; Avcıoğlu, E. Ambient Relative Humidity Effects on Mechanical Properties of FDM 3D Printed PLA Components. *Phys. Scr.* **2023**, *98*, doi:10.1088/1402-4896/accfcf.
13. Soleyman, E.; Rahmatabadi, D.; Soltanmohammadi, K.; Aberoumand, M.; Ghasemi, I.; Abrinia, K.; Baniassadi, M.; Wang, K.; Baghani, M. Shape Memory Performance of PETG 4D Printed Parts under Compression in Cold, Warm, and Hot Programming. *Smart Mater. Struct.* **2022**, *31*, 085002, doi:10.1088/1361-665X/AC77CB.
14. Hearon, K.; Singhal, P.; Horn, J.; Small, W.; Olsovsky, C.; Maitland, K.C.; Wilson, T.S.; Maitland, D.J. Porous Shape-Memory Polymers. *Polym. Rev.* **2013**, *53*, 41–75, doi:10.1080/15583724.2012.751399.
15. Akman, R.; Ramaraju, H.; Hollister, S.J. Development of Photocrosslinked Poly(Glycerol Dodecanedioate)—A Biodegradable Shape Memory Polymer for 3D-Printed Tissue Engineering Applications. *Adv. Eng. Mater.* **2021**, *23*, 2100219, doi:10.1002/ADEM.202100219.
16. Shirzad, M.; Zolfagharian, A.; Matbouei, A.; Bodaghi, M. Design, Evaluation, and Optimization of 3D Printed Truss Scaffolds for Bone Tissue Engineering. *J. Mech. Behav. Biomed. Mater.* **2021**, *120*, 104594, doi:10.1016/j.jmbbm.2021.104594.
17. Oladapo, B.I.; Ismail, S.O.; Zahedi, M.; Khan, A.; Usman, H. 3D Printing and Morphological Characterisation of Polymeric Composite Scaffolds. *Eng. Struct.* **2020**, *216*, 110752,

doi:10.1016/J.ENGSTRUCT.2020.110752.

18. Ciobanu, R.C.; Schreiner, C.; Aradoaei, M.; Hitruc, G.E.; Rusu, B.-G.; Aflori, M. Characteristics of Composite Materials of the Type: TPU/PP/BaTiO3 Powder for 3D Printing Applications. *Polym. 2023, Vol. 15, Page 73* **2022**, *15*, 73, doi:10.3390/POLYM15010073.

19. Maiti, A.; Small, W.; Lewicki, J.P.; Weisgraber, T.H.; Duoss, E.B.; Chinn, S.C.; Pearson, M.A.; Spadaccini, C.M.; Maxwell, R.S.; Wilson, T.S. 3D Printed Cellular Solid Outperforms Traditional Stochastic Foam in Long-Term Mechanical Response. *Sci. Rep.* **2016**, *6*, doi:10.1038/srep24871.

20. Kashyap, D.; Kishore Kumar, P.; Kanagaraj, S. 4D Printed Porous Radiopaque Shape Memory Polyurethane for Endovascular Embolization. *Addit. Manuf.* **2018**, *24*, 687–695, doi:10.1016/j.addma.2018.04.009.

21. Chevalier, E.; Chulia, D.; Pouget, C.; Viana, M. Fabrication of Porous Substrates: A Review of Processes Using Pore Forming Agents in the Biomaterial Field. *J. Pharm. Sci.* **2008**, *97*, 1135–1154, doi:10.1002/JPS.21059.

22. Sadegh Ebrahimi, M.; Hashemi, R.; Etemadi, E. In-Plane Energy Absorption Characteristics and Mechanical Properties of 3D Printed Novel Hybrid Cellular Structures. *J. Mater. Res. Technol.* **2022**, *20*, 3616–3632, doi:10.1016/J.JMRT.2022.08.064.

23. Uribe-Lam, E.; Treviño-Quintanilla, C.D.; Cuan-Urquizo, E.; Olvera-Silva, O. Use of Additive Manufacturing for the Fabrication of Cellular and Lattice Materials: A Review. *Mater. Manuf. Process.* 2021, *36*.

24. Kumar, V.; Singh, R.; Ahuja, I.S. On Programming of Polyvinylidene Fluoride–Limestone Composite for Four-Dimensional Printing Applications in Heritage Structures. *https://doi.org/10.1177/14644207211044298* **2021**, *236*, 319–333, doi:10.1177/14644207211044298.

25. Xu, Y.; Zhang, F.; Zhai, W.; Cheng, S.; Li, J.; Wang, Y. Unraveling of Advances in 3D-Printed Polymer-Based Bone Scaffolds. *Polym. 2022, Vol. 14, Page 566* **2022**, *14*, 566, doi:10.3390/POLYM14030566.

26. Huang, X.; Panahi-Sarmad, M.; Dong, K.; Cui, Z.; Zhang, K.; Gelis Gonzalez, O.; Xiao, X. 4D Printed TPU/PLA/CNT Wave Structural Composite with Intelligent Thermal-Induced Shape Memory Effect and Synergistically Enhanced Mechanical Properties. *Compos. Part A Appl. Sci. Manuf.* **2022**, *158*, doi:10.1016/j.compositesa.2022.106946.

27. Song, D.; Chen, X.; Wang, M.; Wu, Z.; Xiao, X. 3D-Printed Flexible Sensors for Food Monitoring. *Chem. Eng. J.* **2023**, *474*, 146011, doi:10.1016/J.CEJ.2023.146011.

28. Cao, M.; Cui, T.; Yue, Y.; Li, C.; Guo, X.; Jia, X.; Wang, B. Preparation and Characterization for the Thermal Stability and Mechanical Property of PLA and PLA/CF Samples Built by FFF Approach. *Mater. 2023, Vol. 16, Page 5023* **2023**, *16*, 5023, doi:10.3390/MA16145023.

29. Carrell, J.; Gruss, G.; Gomez, E. Four-Dimensional Printing Using Fused-Deposition Modeling: A Review. *Rapid Prototyp. J.* **2020**, *26*, 855–869, doi:10.1108/RPJ-12-2018-0305/FULL/XML.

30. Kechagias, J.; Chaidas, D.; Vidakis, N.; Salonitis, K.; Vaxevanidis, N.M. Key Parameters Controlling Surface Quality and Dimensional Accuracy: A Critical Review of FFF Process. *Mater. Manuf. Process.* 2022, *37*.

31. Mogan, J.; Harun, W.S.W.; Kadirgama, K.; Ramasamy, D.; Foudzi, F.M.; Sulong, A.B.; Tarlochan, F.; Ahmad, F. Fused Deposition Modelling of Polymer Composite: A Progress. *Polym. 2023, Vol. 15, Page 28* **2022**, *15*, 28, doi:10.3390/POLYM15010028.

32. Mohol, S.S.; Sharma, V. Functional Applications of 4D Printing: A Review. *Rapid Prototyp. J.* **2021**, *27*, 1501–1522, doi:10.1108/RPJ-10-2020-0240/FULL/XML.

33. Soleyman, E.; Aberoumand, M.; Rahmatabadi, D.; Soltanmohammadi, K.; Ghasemi, I.; Baniassadi, M.; Abrinia, K.; Baghani, M. Assessment of Controllable Shape Transformation, Potential Applications, and Tensile Shape Memory Properties of 3D Printed PETG. *J. Mater. Res. Technol.* **2022**, *18*, 4201–4215, doi:10.1016/J.JMRT.2022.04.076.

34. Hamzehei, R.; Serjouei, A.; Wu, N.; Zolfagharian, A.; Bodaghi, M. 4D Metamaterials with Zero Poisson's Ratio, Shape Recovery, and Energy Absorption Features. *Adv. Eng. Mater.* **2022**,

2200656, doi:10.1002/ADEM.202200656.

35. Piorkowska, E.; Kulinski, Z.; Galeski, A.; Masirek, R. Plasticization of Semicrystalline Poly(l-Lactide) with Poly(Propylene Glycol). *Polymer (Guildf).* **2006**, *47*, 7178–7188, doi:10.1016/J.POLYMER.2006.03.115.

36. Rahmatabadi, D.; Ghasemi, I.; Baniassadi, M.; Abrinia, K.; Baghani, M. 3D Printing of PLA-TPU with Different Component Ratios: Fracture Toughness, Mechanical Properties, and Morphology. *J. Mater. Res. Technol.* **2022**, *21*, 3970–3981, doi:10.1016/j.jmrt.2022.11.024.

37. Zhang, J.; Zhang, X.; Wang, Z. zhang; Li, H. yu An Experimental and Modeling Investigation on the Effects of Temperature and Strain Rate on the Tensile-Deformation Behavior of TB991 Weld Sealant. *Mech. Time-Dependent Mater.* **2022**, doi:10.1007/s11043-021-09536-7.

38. Aberoumand, M.; Soltanmohammadi, K.; Soleyman, E.; Rahmatabadi, D.; Ghasemi, I.; Baniassadi, M.; Abrinia, K.; Baghani, M. A Comprehensive Experimental Investigation on 4D Printing of PET-G under Bending. *J. Mater. Res. Technol.* **2022**, *18*, 2552–2569, doi:10.1016/J.JMRT.2022.03.121.

39. Tobushi, H.; Hayashi, S.; Hoshio, K.; Miwa, N. Influence of Strain-Holding Conditions on Shape Recovery and Secondary-Shape Forming inpolyurethane-Shape Memory Polymer. *Smart Mater. Struct.* **2006**, *15*, 1033, doi:10.1088/0964-1726/15/4/016.

40. Tobushi, H.; Matsui, R.; Hayashi, S.; Shimada, D. The Influence of Shape-Holding Conditions on Shape Recovery of Polyurethane-Shape Memory Foams. *Smart Mater. Struct.* **2004**, *13*, 881, doi:10.1088/0964-1726/13/4/026.

41. Gurrala, P.K.; Regalla, S.P. Part Strength Evolution with Bonding between Filaments in Fused Deposition Modelling. *http://dx.doi.org/10.1080/17452759.2014.913400* **2014**, *9*, 141–149, doi:10.1080/17452759.2014.913400.

42. Seppala, J.E.; Hoon Han, S.; Hillgartner, K.E.; Davis, C.S.; Migler, K.B. Weld Formation during Material Extrusion Additive Manufacturing. *Soft Matter* **2017**, *13*, 6761–6769, doi:10.1039/C7SM00950J.

43. Rahmatabadi, D.; Soltanmohammadi, K.; Aberoumand, M.; Soleyman, E.; Ghasemi, I.; Baniassadi, M.; Abrinia, K.; Bodaghi, M.; Baghani, M. Development of Pure Poly Vinyl Chloride (PVC) with Excellent 3D Printability and Macro- and Micro-Structural Properties. *Macromol. Mater. Eng.* **2023**, *308*, 2200568, doi:10.1002/mame.202200568.

44. Bhalodi, D.; Zalavadiya, K.; Gurrala, P.K. Influence of Temperature on Polymer Parts Manufactured by Fused Deposition Modeling Process. *J. Brazilian Soc. Mech. Sci. Eng. 2019 413* **2019**, *41*, 1–11, doi:10.1007/S40430-019-1616-Z.

45. Rahmatabadi, D.; Aberoumand, M.; Soltanmohammadi, K.; Soleyman, E.; Ghasemi, I.; Baniassadi, M.; Abrinia, K.; Bodaghi, M.; Baghani, M. Toughening PVC with Biocompatible PCL Softeners for Supreme Mechanical Properties, Morphology, Shape Memory Effects, and FFF Printability. *Macromol. Mater. Eng.* **2023**, 2300114, doi:10.1002/MAME.202300114.